Core-hole spectator Auger decay

K. Jänkälä,[1] P. Lablanquie,[2] L. Andric,[2] M. A. Khalal,[2] J. Palaudoux,[2] F. Penent,[2] J.-M. Bizau,[3,4] D. Cubaynes,[3,4] S. Guilbaud,[3] K. Ito,[4] K. Bučar,[5] M. Žitnik,[5] M. Huttula,[1] T. Kaneyasu,[6] and Y. Hikosaka[7]

[1]*Nano and Molecular Systems Research Unit, University of Oulu, P.O. Box 3000, 90014 Oulu, Finland*

[2]*Sorbonne Université, CNRS, Laboratoire de Chimie Physique-Matière et Rayonnement, 4 Place Jussieu, 75005 Paris, France*

[3]*ISMO, CNRS UMR 8214, Université Paris-Sud, Université Paris-Saclay, 91405 Orsay, France*

[4]*Synchrotron SOLEIL, l'Orme des Merisiers, Saint-Aubin, Boîte Postale 48, 91192 Gif-sur-Yvette Cedex, France*

[5]*Jozef Stefan Institute, Jamova Cesta 39, SI-1001 Ljubljana, Slovenia*

[6]*SAGA Light Source, Tosu 841-0005, Japan*

[7]*Institute of Liberal Arts and Sciences, University of Toyama, 930-0194, Japan*

(Received 18 September 2019; accepted 22 January 2020; published 26 February 2020)

For an atomic state with two electrons missing from different core orbitals one may assume that the deeper hole decays first. However, it is quite probable that the double core-hole state will decay by emission of a slow Auger electron where the deeper core hole remains a spectator, especially if the outer core hole can be filled by Coster-Kronig transition, while the deeper cannot. We study here the competition of both Auger decay channels in a model system, the $1s2s2p^6(3s/3p)$ states of Ne^+ ions. As the phenomenon can take place in any decay chain involving multiple core-excited states it can be critical to understand the ion yields, the electron and x-ray emission spectra, and the molecular fragmentation.

DOI: 10.1103/PhysRevA.101.023413

I. INTRODUCTION

Auger electron spectroscopy (AES) is based on a process where a hole in an electronic inner-shell orbital is filled by an electron from an outer orbital while a second electron (the Auger electron) is emitted into the continuum. The kinetic energy of the emitted electron is given by the energy difference between the initial and final states of the transition. The basic Auger effect is thus a two-electron process arising from electron correlations, and for decades AES has been developed as an instrumental tool in materials science ranging from studies of single atoms to surface sciences (see, e.g., Refs. [1–3] and references therein).

Traditionally AES studies have relied on the creation of a single initial hole, but recent developments in high-efficiency multielectron coincidence detection techniques have highlighted unique aspects to the process. For example, it has become possible to study Auger emission from one-site [4–8] and two-site double core holes [9], and to follow Auger decay cascades [10–14] and weak many-electron Auger processes [13–19].

In this study we focus on the Auger decay of two-hole states in a case where two holes lay in two different suborbitals. Such states can be produced directly in single-photon excitation at synchrotrons, by multiphoton processes at x-ray free-electron lasers (FELs), or by electron or ion bombardment. These states can be also prepared indirectly via Auger decay cascades because, if the initial single hole is at a deep enough orbital, the system may undergo several Auger decay steps where the ionization state of the system is increased by 1 at each step.

The question we address in the paper is, how do such two-hole states decay? If the holes are at the same orbital one can expect that the state decays roughly 2–3 times faster than the corresponding one-hole state [7,20] and that this factor decreases when the nuclear charge increases [21]. On the other hand, what happens if the holes are in different orbitals? The most common answer is probably that the state prefers to decay by filling the deeper hole first with a decay time that is roughly the same as for the state without the outer hole. This assumption arises from the usual behavior of ionic states, since one can argue that in general the deeper the hole, the larger the possible decay channels are and the more unstable the state is. There can be, however, a drastic contrast to such assumption. It is possible that the outer hole is filled first with emission of a slow Auger electron, even if the deeper hole is in the *K* shell. In the present paper this process is denoted as core spectator Auger (CSA) decay and the process where the deeper hole is filled first as core participator Auger (CPA) decay. We argue that the branching ratio for decay via the CSA or CPA path depends on the positions of the holes and that if the shallower hole can decay via Coster-Kronig (C-K) or super C-K transition [22] but the deeper cannot, the CSA path may be very intense and may even be the dominant decay process.

The interplay between Auger decay paths of two-hole configurations was discussed in the context of Ar^+ $2p^{-1}3s^{-1}4s$ states in Ref. [11], where a decay into the Ar^{2+} $2p^{-1}3p^{-1}$ states was indeed observed. However, the competition with the CPA path and the generality of such processes were not addressed. Here, we show that CSA decay may be intense even if the binding energies of the orbitals differ by nearly two orders of magnitude.

In the present paper we study in detail the competition of the CSA and CPA paths. As systems with two asymmetric deep core holes are hard to reach experimentally with

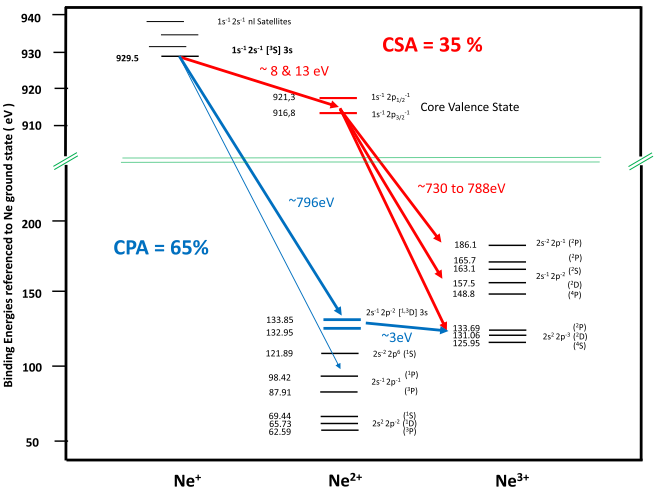

FIG. 1. Schematic representation of CSA and CPA paths following the decay of the Ne^+ $1s2s[^3S]2p^63s$ shake-up satellite. Note that for visibility the energy axis is divided into two regions, and a different y-axis scaling is used above and below the break. The corresponding paths for the $1s2s[^1S]2p^63s$ state are similar (except that first step CSA and CPA Auger electrons have then, respectively, 14 & 19 eV, and 802 eV). Energy levels are from NIST tables, except for the levels displayed as red and blue bars which are obtained from our experiment.

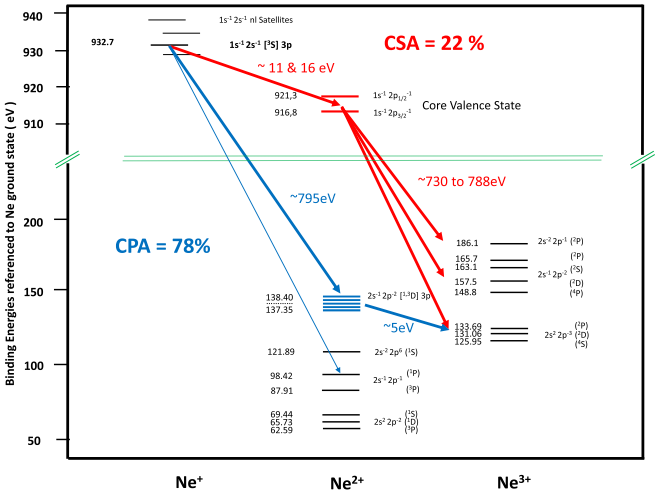

FIG. 2. Schematic representation of CSA and CPA paths following the decay of the Ne^+ conjugate shake-up satellite $1s2s[^3S]2p^63p$. It is similar to Fig. 1 which describes the decay of the Ne^+ normal shake-up satellite. The corresponding paths for the $1s2s[^1S]2p^63p$ state are similar (except that first step CSA and CPA Auger electrons have then, respectively, 17 & 22 eV, and 801 eV).

our method, we consider here as a model system the Ne^+ $1s^{-1}(2s \rightarrow 3s/3p)$ photoionization shake-up satellite states. They present two holes, one in the deep $1s$ core shell and one in the $2s$ inner valence shell. Note that both holes (whether the $1s^{-1}$ or the $2s^{-1}$ one), if alone, would Auger decay.

The singly ionized two-hole configurations, $1s2s2p^6(3s/3p)$, have two possible Auger decay pathways. One is that the $1s$ hole is filled first, leading to the CPA path with emission of an electron with kinetic energy of about 800 eV. In the second path the $2s$ hole is filled first by a Coster-Kronig process involving a $2p$ electron while an outer $3s/3p$ electron is emitted (or vice versa, although the overlap of the $2p$ electron with the $2s$ hole favors the first image), thus leading to the CSA path with emission of an electron with a kinetic energy of about 10 eV. The CSA and CPA decays are shown in Eq. (1) and depicted in Fig. 1 for the $1s2s[^3S]2p^63s$ state plus Fig. 2 for the $1s2s[^3S]2p^63p$ state,

$$
\begin{aligned}
&h\nu + \mathrm{Ne} \rightarrow \mathrm{Ne}^+ 1s2s2p^6(3s/3p) + e_p^- \\
&\mathrm{CSA} \rightarrow \mathrm{Ne}^{2+} 1s2s^22p^5 + e_{\mathrm{CSA}}^- \quad (\sim 10\,\mathrm{eV}) \\
&\qquad \rightarrow \mathrm{Ne}^{3+} 1s^22s^22p^3 + e^- \quad (\sim 800\,\mathrm{eV}) \\
&\text{or} \\
&\mathrm{CPA} \rightarrow \mathrm{Ne}^{2+} 1s^22s2p^4(3s/3p) + e_{\mathrm{CPA}}^- \quad (\sim 800\,\mathrm{eV})
\end{aligned}
\tag{1}
$$

After CSA decay, the Ne^{2+} ion is still in a highly unstable state with a hole in a $1s$ orbital that decays further via emission of a second Auger electron, as shown in Fig. 1. The full decay path thus consists of emission of a slow Auger electron (CSA) followed by a fast electron. The fast electron falls roughly to the same kinetic energy range as the first electron in the CPA path.

As for the CPA path, depending on the Ne^{2+} final state populated in the decay of the $1s$ hole, the fast electron can be followed (or not, depending on the state) by a slow one to end up with a Ne^{3+} (or Ne^{2+}) state. In the following, red is used to indicate the CSA first path and blue the CPA first path.

II. EXPERIMENT

The experiment was carried out at the SEXTANT beamline [23] of the 2.75 GeV synchrotron storage ring SOLEIL in St. Aubin, France. The ring was operated in single-bunch mode, providing x-ray light pulses every 1.184 μs. The measurements were performed using a magnetic-bottle time-of-flight (MB-TOF) spectrometer. An 80-kHz mechanical chopper was used to extend the pulse period up to $\sim$12 μs in order to allow measurement of the absolute electron flight times [24]. In addition, preliminary measurements were performed at the beamline BL-16A of the Photon Factory (Tsukuba, Japan) using the same type of experimental arrangement.

The MB-TOF instrument is described in detail in Ref. [18]. The setup is composed of a combination of a strong (0.7 T) and inhomogeneous magnetic field from a permanent magnet near the ionization volume and a weak (1 mT) and uniform magnetic field created by a 2-m-long solenoid. The combined fields form a magnetic mirror that collects electrons from the ionization region and guides them onto a microchannel plate detector at the end of the flight tube. A time-to-digital converter is used to measure the arrival times of the electrons with respect to the synchrotron ring clock. The instrument has relative resolution of $\Delta E/E \sim 1.6\%$ and a detection efficiency which decreases with electron kinetic energy (of 55% 47%, and 17% for $E = 10$, 200, and 800 eV, respectively). The photon energy was set to 965 eV with an approximate resolution of 150 meV.

III. THEORY

The calculations were done in relativistic configuration interaction Dirac-Fock framework (see, e.g., [25]) using the GRASP2K code [26] with a Dirac-Coulomb Hamiltonian and jj-coupled configuration state function basis. For simplicity the number of states and configurations was kept as small as possible by including only configurations listed in Fig. 1. The $3p$ case was calculated in the same way, except that the $3s$ orbital was replaced by $3p$. The CSA and CPA decay rates were calculated using the Auger component of the RATIP package [27]. Photoionization to the Ne^+ $1s^{-1}2s^{-1}(3s/3p)$ states was treated using a modified version of the PHOTO component of RATIP, which provides a rough estimate for the cross sections based on the sudden approximation [28,29].

IV. RESULTS AND DISCUTION

A. Competition between core-hole spectator (CSA) and core-hole participant (CPA) Auger decays

Figure 3(b) shows the K-shell photoelectron spectrum of Ne. The $1s$ photoelectron line appears at about 95 eV. It is followed at lower kinetic energies (∼48–58 eV) by the Ne^+ $1s^{-1}2p^{-1}nl$ satellite lines for which the CSA path is closed and by the $1s^{-1}2p^{-1}nl$ satellite lines (∼25–35 eV) which are of interest here. Four peaks are distinguished here; they correspond to the monopole $1s2s[^{1,3}S]2p^63s$ and conjugate $1s2s[^{1,3}S]2p^63p$ shake-up states. The two-dimensional maps of all coincidence pairs in Fig. 3 show fast (panel A) and slow (panel C) Auger electrons coincident with the different photoelectrons. For the $1s$ photoelectron single Auger decay produces fast Auger electrons while slow Auger electrons correspond to double Auger decay of the $1s$ hole [27,30]. The decay of the Ne^+ $1s^{-1}2p^{-1}nl$ satellite states produces a complex structure of low-energy cascade Auger electrons as studied in [13]. The low-energy Auger electrons observed in coincidence with the $1s^{-1}2s^{-1}nl$ photoelectrons allow us to separate unambiguously the CSA and CPA paths:

The CSA path populates the Ne^{2+} $1s2s^22p^5$ ($^{1,3}P$) states. These two states are also formed by direct double photoionization as evidenced by the two diagonal lines in Fig. 3(c), associated to the coincidence detection of the two photoelectrons emitted from the $1s$ and $2p$ orbitals [31]. Therefore, the CSA path induces Fano profiles due to interferences between the sequential and direct paths:

$$\begin{array}{ccc} & \nearrow & Ne^+\ 1s^{-1}2s^{-1}(3s/3p) + e^-_p \\ h\nu + Ne & \longrightarrow & \\ & \searrow & Ne^{2+}\ 1s2s^22p^5\ (^{1,3}P) + 2\ e^-_p \end{array} . \qquad (2)$$

This interference process has been observed experimentally in photoelectron spectra [32,33], and has also attracted theoretical interest [34,35]. The coincidence method allows the separation of the two Ne^{2+} $1s2s^22p^5$ (^1P) and (^3P) channels in finer detail than in the previous study [31]. We confirm, for instance, the prediction [35] that the Ne^+ $1s2s[^3S]2p^63s$ state decays preferably to the Ne^{2+} $1s2s^22p^5$ (^1P) state, rather than to the (^3P) one.

The CPA path is revealed in Fig. 3(c) by the second step slow Auger electrons emitted at kinetic energy of about

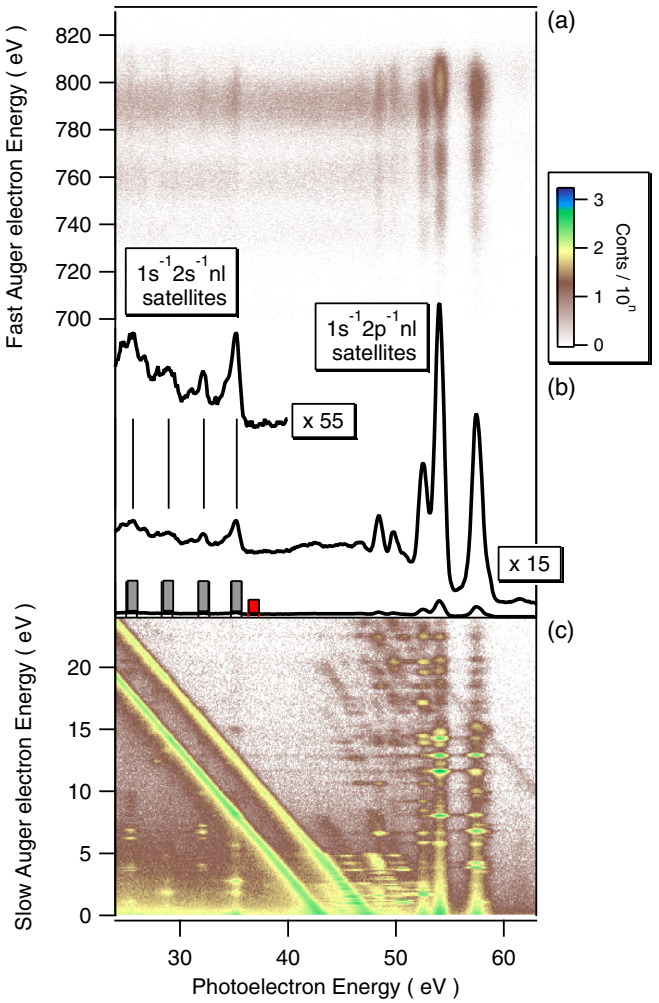

FIG. 3. Fast and slow Auger decays of Ne $1s$ satellites. (b) is the photoelectron spectrum. The two-dimensional (e, e) coincidence maps reveal the detection of the fast (a) and slow (c) Auger electron in coincidence with their associated photoelectron. The gray and red zones highlighted in (b) show the energy ranges used for the true and false coincidence spectra in Fig. 4.

1–10 eV after release of the ∼800-eV CPA Auger electron (see Fig. 1); these are both observed in coincidence with the $1s^{-1}2s^{-1}nl$ photoelectrons. Integration over the slow-energy Auger electrons in Fig. 3(c) (excluding the diagonal lines of the CSA path) is depicted by the uppermost spectrum in Fig. 4. It gives the intensity of the CPA path for each Ne^+ $1s^{-1}2s^{-1}nl$ satellite state.

The branching ratio between the CPA and CSA paths can be quantified from Fig. 4. Results are given in Table I. The large error bars (±10%) are due mainly to the estimate of the resonant contribution (CSA path) to the Fano profiles. The table shows also the results of two theoretical approaches. A simple model considers that the $1s^{-1}$ and $2s^{-1}$ holes of the Ne^+ $1s^{-1}2s^{-1}nl$ satellite state will decay with the probability proportional to the lifetimes of the single holes, Ne $1s^{-1}2s^22p^6nl$ and $1s^22s^{-1}2p^6nl$ (as calculated here). This model gives the correct order of magnitude for the CSA/CPA branching ratio but fails to predict its dependence with the $1s^{-1}2s^{-1}$ $[^{1,3}S]$ core coupling. Our detailed calculations

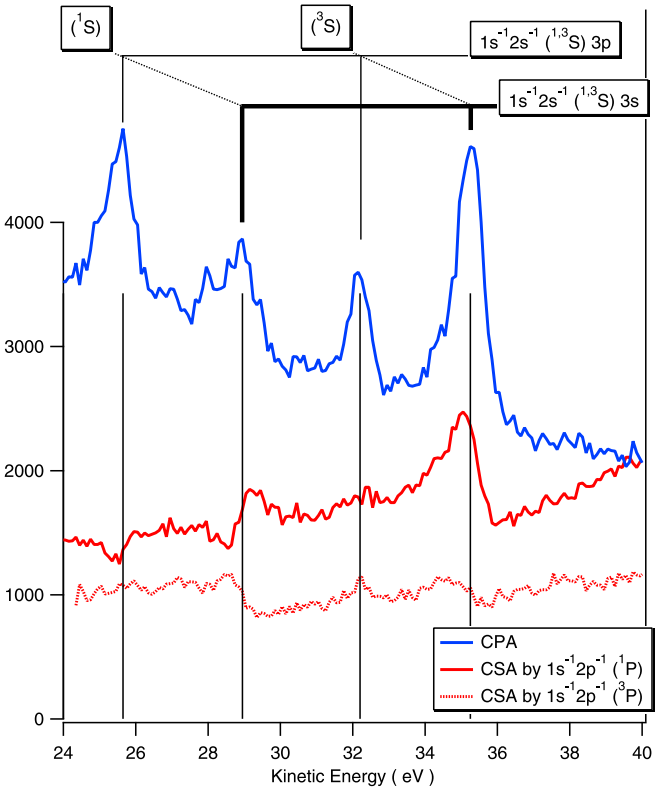

FIG. 4. Comparison of the relative probabilities of the CPA and CSA paths, deduced from Fig. 3. The CSA paths through the $Ne^{2+}1s2s2p^5$ (^3P) and (^1P) paths are differentiated. See text for details.

confirm this dependence but overestimate the CSA decay probability.

B. Intermediate Ne^{2+} states populated in the CPA decay are above Ne^{3+} threshold

To locate the Ne^{2+} states populated in the CPA decay we examine first the fast Auger electrons. Figure 5 deals with the decay of the Ne^+ $1s2s[^3S]2p^63s$ shake-up state while Fig. 6 deals with that of the Ne^+ $1s2s[^3S]2p^63p$ conjugate shake-up state. Figure 5 shows the Auger spectra measured in coincidence with the $1s^{-1}$ photoelectron [Fig. 5(a)] or the $1s2s[^3S]2p^63s$ one [Fig. 5(b)]. They are plotted as a function of binding energy of the populated Ne^{2+} states by referencing the ∼800 eV Auger electrons with respect to the Ne^+ initial states. The resolution of these experimental spectra is governed by that of the ∼800-eV electrons and is estimated to ∼13 eV. We observe that the CPA decay of the $1s2s[^3S]2p^63s$ satellite states populates essentially highly excited Ne^{2+} states positioned above the Ne^{3+} threshold. The present calculation is depicted in Fig. 5(c). Comparison with experiment shows good agreement and suggests Ne^{2+} $1s^22s2p^4[^{2,4}D]3s$ as intermediate states, as will be confirmed below. Our experiment in Fig. 5(b), supported by calculation, reveals also a weak population of lower-lying Ne^{2+} states of ∼90 eV binding energy and of $1s^22s2p^5(^{3,1}P)$ configuration, associated with faster Auger electrons of ∼840 eV. These cannot decay further by electron emission because they are located below the Ne^{3+} threshold.

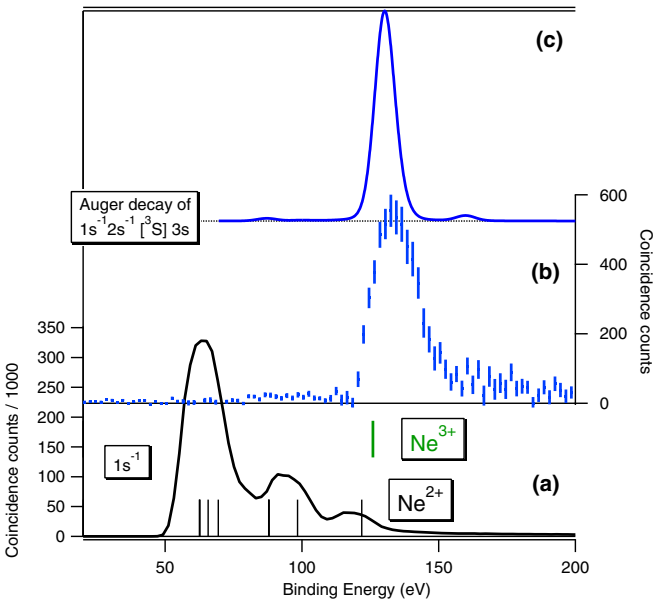

FIG. 5. Ne^{2+} states populated by the Auger decay of the Ne^+ $1s^{-1}$ state (a) or by CPA decay of the Ne^+ $1s2s[^3S]2p^63s$ state [(b) is experiment, (c), our calculation]. Experimental curves are obtained from the Auger spectra observed in coincidence with the corresponding photoelectrons, in the energy range defined in Fig. 3(b) by the gray rectangles. Conversion of the $E_A \sim 800$ eV fast Auger electron energies into binding energy B_{En} of the Ne^{2+} states populated by the Auger decay is given by $B_{En} = B_E^+ - E_A$ where B_E^+ is the binding energy of the initial hole state. Vertical lines indicate Ne^{2+} levels and Ne^{3+} threshold from the NIST database. Note that for (b) false coincidences have been subtracted; they are estimated from coincidences with electrons in the red zone in Fig. 3(b) and contain also an estimate of the pollution by the core valence direct double photoionization path (2). The resulting spectrum in (b) includes a weak contribution of the fast Auger electrons emitted in the second step CSA decay; however, their lower kinetic energies than the first step CPA electrons convert into a contribution and an asymmetry on the high binding energy side of the experimental peak.

TABLE I. Probability (in percent) for the $1s^{-1}2s^{-1}[^{1,3}S]nl$ states to decay by core spectator Auger decay. The simple model predicts that the $1s^{-1}$ and $2s^{-1}$ holes will decay with a probability described by the calculated lifetimes of the $1s^{-1}2s^22p^6nl$ (320 meV for $nl = 3s$ and 276 meV for $3p$) and $1s^22s^{-1}2p^6nl$ levels (148 meV for $3s$ and 18 meV for $3p$).

Ne^+ state	$(^3S)3s$	$(^1S)3s$	$(^3S)3p$	$(^1S)3p$
Experiment (±10)	35	33	22	4
Simple model	31	31	6	6
This calculation	66.1	51.0	36.8	14.9

C. Assignment of the intermediate Ne^{2+} states populated in the CPA decay

We saw that most of the intermediate Ne^{2+} states populated in the CPA decay will further decay to Ne^{3+}. By referencing the second step Auger electrons to the final Ne^{3+} states it is possible to define the Ne^{2+} intermediates states with high resolution and even observe their lifetime broadening:

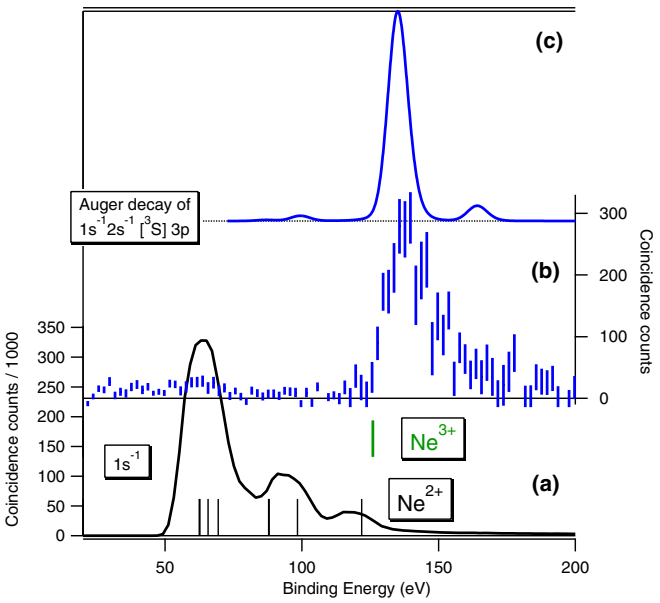

FIG. 6. Equivalent of Fig. 5 but for the Ne^+ conjugate shake-up satellite $1s2s[^3S]2p^63p$. As for Fig. 5, the experimental CPA Auger spectrum in (b) is obtained from the spectrum of electrons detected in coincidence with the $1s2s[^3S]2p^63p$ photoelectron line, selected in the gray zone of Fig. 3(b). False coincidences and an estimate of the pollution by the direct core valence double ionization to the Ne^{2+} $1s2s^22p^5$ ($^{1,3}P$) states are subtracted. These contributions were estimated from the spectrum of electrons detected in coincidence with electrons selected in the red zone of Fig. 3(b).

Figure 7 (center) shows the spectrum of these low-energy electrons emitted in the decay of each of the two Ne^+ $1s2s[^{1,3}S]2p^63s$ states, while Fig. 8 shows the equivalent for the two Ne^+ $1s2s[^{1,3}S]2p^63p$ states. One recognizes groups of peaks that are separated by the $Ne^{3+}(^2P/^2D)$ splitting. It is thus possible to deduce the position of the Ne^{2+} intermediate states with respect to these Ne^{3+} final states. The result is reported in Table II. Another argument for this assignment is extracted from the three-electron coincidence maps in Figs. 7 and 8 (top and bottom). They show the coincidence map between the two Auger electrons (fast on the y axis and slow on the x axis) detected in coincidence with the associated photoelectron. The red diagonal lines indicate in each spectrum the locations expected for a final Ne^{3+} state of configuration $2s^22p^3(^4S)$, (^2D), (^2P), and $2s2p^4(^4P)$, respectively, from top to bottom.

The assignment of the Ne^{2+} intermediate states is naturally obtained if we consider that in the CPA decay of the Ne^+ $1s2s[^{1,3}S]2p^6(3s/3p)$ states, the outer $3s$ or $3p$ electron remains a spectator during the $1s^{-1}$ core-hole decay. As the Auger decay of the Ne^+ $1s^{-1}$ hole populates mainly the $Ne^{2+}2p^{-2}$ (^1D) state, it is natural to propose that the dominant CPA decay populates the Ne^{2+} $1s^22s2p^4[^{2,4}D](3s/3p)$ states. Such an assignment is confirmed by our calculations.

It is also interesting to observe in Fig. 7 that the peak widths of the electrons emitted in the decay of the Ne^{2+} $1s^22s2p^4[^{2,4}D]3s$ sates are broader than those for the decay of the Ne^{2+} $1s^22s2p^4[^{2,4}D]3p$ states (Fig. 8). We observe a Lorentzian broadening of ∼240 meV in the first case, while in the second case peak widths are ∼60 meV which is the experimental resolution. This reveals the shorter lifetime of the Ne^{2+} $1s^22s2p^4[^{2,4}D]3s$ states compared to the Ne^{2+} $1s^22s2p^4(^{2,4}D)3p$ ones, because an outer $3s$ electron fills in the $2s$ hole more easily than a $3p$ one.

From Figs. 7 and 8 we also extract the relative branching ratios for the CPA decay of each Ne^+ $1s2s[^{1,3}S]2p^6(3s/3p)$ state. They are reported in Table II. Selectivity is observed in the decay path. One notices, for instance, that the Ne^{2+} d state of $1s^22s2p^4[^{2,4}D]3p$ configuration decays to the Ne^{3+} $2p^3$ (^2D) final state but not to the Ne^{3+} $2p^3$ (^2P) one. The origin lies probably in the exact term value of the Ne^{2+} d state, and in propensity rules for its decay.

TABLE II. Binding energies of the Ne^{2+} intermediate states involved in the CPA decay, deduced from Figs. 7 and 8 and referenced to the Ne ground state. Then, for each Ne^+ $1s2s[^{1,3}S]2p^6(3s/3p)$ state, the branching ratio (in percent) for the decay to the Ne^{3+} $2p^3(^2D)$ and Ne^{3+} $2p^3$ (^2D) final states through each of the Ne^{2+} intermediate state is given. "×" denotes that this channel is closed.

	$1s^22s2p^4[^{2,4}D]3s$		$1s^22s2p^4[^{2,4}D]3p$				
Ne^{2+} state	*A*	*B*	*a*	*b*	*c*	*d*	*e*
Binding energy (eV)	132.95	133.95	137.35	137.58	137.80	138.00	138.40
Decay of $Ne^+[^3S]3s$							
to Ne^{3+} $2p^3(^2D)$	20	50					
to Ne^{3+} $2p^3(^2P)$	×	30					
Decay of Ne^+ $[^1S]3s$							
to Ne^{3+} $2p^3(^2D)$	100	0					
to Ne^{3+} $2p^3(^2P)$	×	0					
Decay of $Ne^+[^3S]3p$							
to Ne^{3+} $2p^3(^2D)$			10	0	25	15	20
to Ne^{3+} $2p^3(^2P)$			10	5	10	0	5
Decay of $Ne^+[^1S]3p$							
to Ne^{3+} $2p^3$ (^2D)			30	0	5	18	5
to Ne^{3+} $2p^3$ (^2P)			18	18	5	0	0

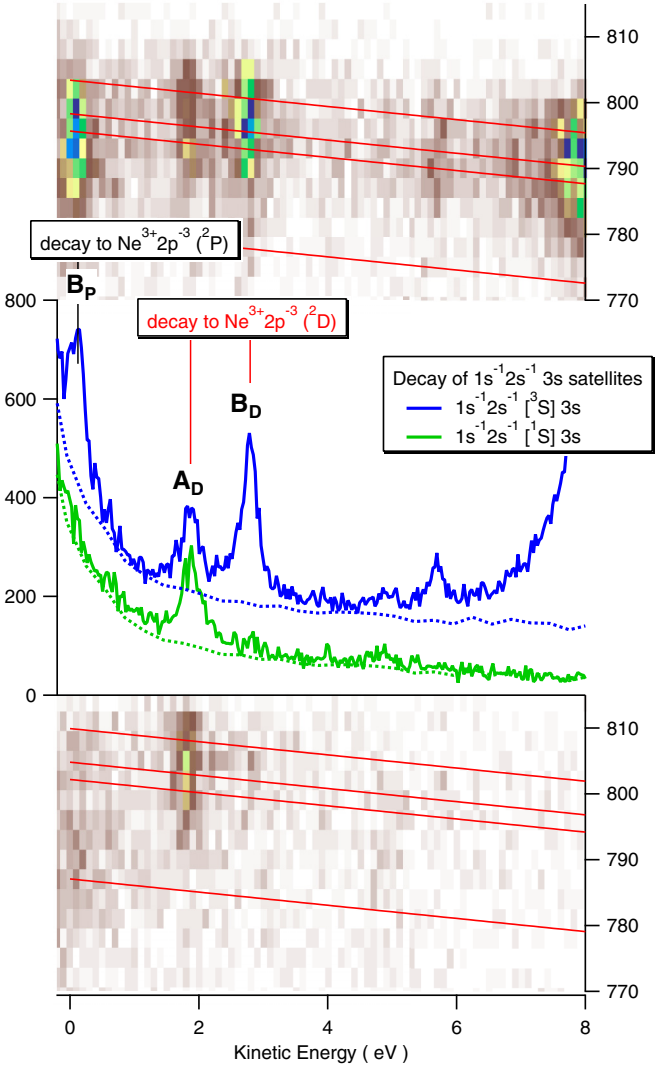

FIG. 7. Center: Spectra of the low-energy electrons emitted upon Auger decay of the Ne^+ $1s2s[^{1,3}S]2p^63s$ state. The dotted lines indicate an estimate of the background of false coincidences, obtained from coincidences with electrons in the red zone of Fig. 3(b). A vertical offset of 100 is used for the upper curves to separate them from the lower ones. Top and bottom show the energy correlation map between the slow (x axis) and the fast (y axis) Auger electrons detected in coincidence with the Ne^+ $1s2s[^3S]2p^63s$ photoelectron (top) or with the one Ne^+ $1s2s[^1S]2p^63s$ photoelectron (bottom).

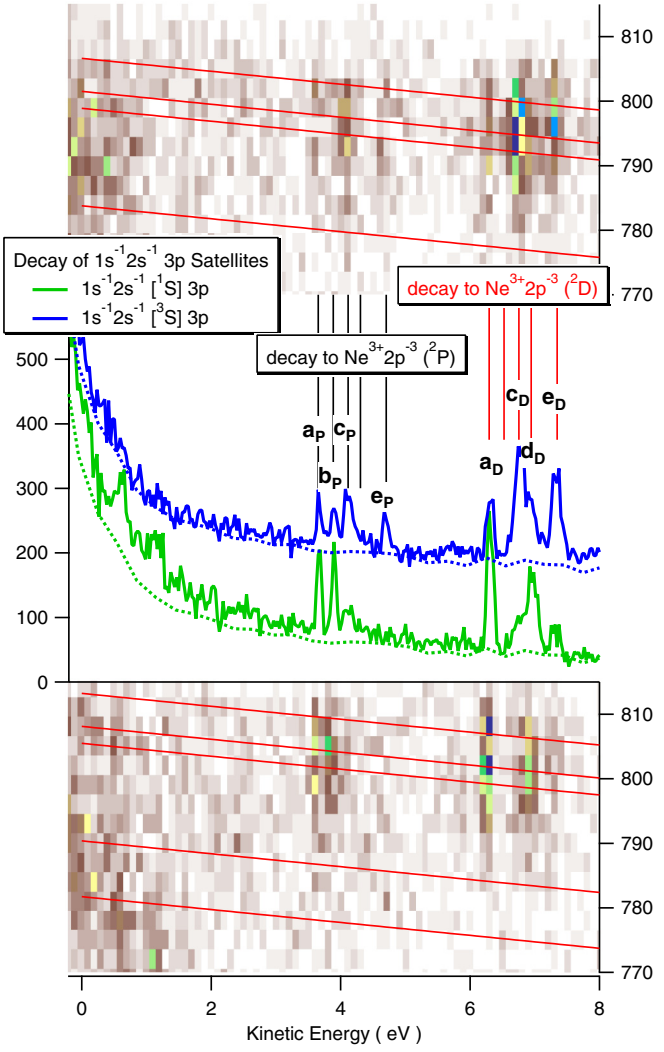

FIG. 8. Center: Spectra of the low-energy electrons emitted upon Auger decay of the Ne^+ $1s2s[^{1,3}S]2p^63p$ state. Similar to Fig. 7, the top and bottom maps show the energy correlation maps between the slow (x axis) and the fast (y axis) Auger electrons detected in coincidence with the Ne^+ $1s2s[^3S]2p^63p$ photoelectron (top) or with the one Ne^+ $1s2s[^1S]2p^63p$ photoelectron (bottom).

V. CONCLUSION

In conclusion, a study of the full Auger decay scheme following K-orbital ionization accompanied by inner-valence coexcitation is provided. Our work reveals that the Auger decay of such states can be a complex competition between two channels leading to Auger electrons with kinetic energy difference of almost two orders of magnitude. Counterintuitively, a decay cascade following a two-electron excitation of a system about 1 keV above its ground state may begin with an emission of a very low-energy Auger electron that fills the valence hole, even if the other hole is in the K shell.

This CSA decay is general and can take place in any decay chain of a deep inner-shell hole created by hard x-ray sources. CSA is also expected in x-ray FEL interactions where the incident photon field is intense enough to allow multiphoton processes to excite electrons from multiple orbitals [36,37]. Realizing and accounting for CSA decay is important for understanding ion yields, photoelectron and Auger electron spectra, and molecular fragmentation following core ionization. It is also crucial for a correct determination of the chemical environment from x-ray [38] and electron emission spectra, especially when high-intensity x-ray FEL probe pulses are employed that boost the two-hole photoexcitation probability.

ACKNOWLEDGMENTS

This work has been financially supported by the Research Council for Natural Sciences and Engineering of the Academy of Finland. M.A.K., K.I., and T.K. acknowledge the support of the Labex Plas@Par managed by the Agence Nationale de

la Recherche, as part of the "Programme d'Investissements d'Avenir" under Reference No. ANR-11-IDEX-0004-02. The experiments were performed with the approval of the SOLEIL Peer Review Committee (Project No. 20170434). We are grateful to the SEXTANT and SOLEIL staff for all the help during the experiment.

[1] T. A. Carlson, *Photoelectron and Auger Spectroscopy* (Plenum, New York, 1975).
[2] U. Becker and D. A. Shirley, *VUV and Soft X-Ray Photoionization* (Plenum, New York, 1996).
[3] J. F. Watts and J. Wolstenholme, *An Introduction to Surface Analysis by XPS and AES* (Wiley, New York, 2003).
[4] G. B. Armen, H. Aksela, T. Åberg, and S. Aksela, J. Phys. B: At., Mol. Opt. Phys. **33**, R49 (2000).
[5] P. Lablanquie, F. Penent, J. Palaudoux, L. Andric, P. Selles, S. Carniato, K. Bučar, M. Žitnik, M. Huttula, J. H. D. Eland, E. Shigemasa, K. Soejima, Y. Hikosaka, I. H. Suzuki, M. Nakano, and K. Ito, Phys. Rev. Lett. **106**, 063003 (2011).
[6] M. Tashiro, M. Nakano, M. Ehara, F. Penent, L. Andric, J. Palaudoux, K. Ito, Y. Hikosaka, N. Kouichi, and P. Lablanquie, J. Chem. Phys. **137**, 224306 (2012).
[7] G. Goldsztejn, T. Marchenko, R. Püttner, L. Journel, R. Guillemin, S. Carniato, P. Selles, O. Travnikova, D. Céolin, A. F. Lago, R. Feifel, P. Lablanquie, M. N. Piancastelli, F. Penent, and M. Simon, Phys. Rev. Lett. **117**, 133001 (2016).
[8] T. Marchenko, L. Inhester, G. Goldsztejn, O. Travnikova, L. Journel, R. Guillemin, I. Ismail, D. Koulentianos, D. Céolin, R. Püttner, M. N. Piancastelli, and M. Simon, Phys. Rev. A **98**, 063403 (2018).
[9] M. Nakano, F. Penent, M. Tashiro, T. P. Grozdanov, M. Žitnik, S. Carniato, P. Selles, L. Andric, P. Lablanquie, J. Palaudoux, E. Shigemasa, H. Iwayama, Y. Hikosaka, K. Soejima, I. H. Suzuki, N. Kouchi, and K. Ito, Phys. Rev. Lett. **110**, 163001 (2013).
[10] J. Viefhaus, M. Braune, S. Korica, A. Reinköster, D. Rolles, and U. Becker, J. Phys. B: At., Mol. Opt. Phys. **38**, 3885 (2005).
[11] M. Nakano, Y. Hikosaka, P. Lablanquie, F. Penent, S.-M. Huttula, I. H. Suzuki, K. Soejima, N. Kouchi, and K. Ito, Phys. Rev. A **85**, 043405 (2012).
[12] S.-M. Huttula, P. Lablanquie, L. Andric, J. Palaudoux, M. Huttula, S. Sheinerman, E. Shigemasa, Y. Hikosaka, K. Ito, and F. Penent, Phys. Rev. Lett. **110**, 113002 (2013).
[13] Y. Hikosaka, T. Kaneyasu, P. Lablanquie, F. Penent, and K. Ito, Phys. Rev. A **97**, 023405 (2018).
[14] R. Guillemin, K. Jänkälä, B. C. de Miranda, T. Marin, L. Journel, T. Marchenko, O. Travnikova, G. Goldsztejn, I. Ismail, R. Püttner, D. Céolin, B. Lassalle-Kaiser, M. N. Piancastelli, and M. Simon, Phys. Rev. A **97**, 013418 (2018).
[15] V. I. Klimov, Science **287**, 1011 (2000).
[16] F. Penent, P. Lablanquie, R. I. Hall, J. Palaudoux, K. Ito, Y. Hikosaka, T. Aoto, and J. H. D. Eland, J. Electron Spectrosc. Relat. Phenom. **144–147**, 7 (2005).
[17] E. Andersson, S. Fritzsche, P. Linusson, L. Hedin, J. H. D. Eland, J.-E. Rubensson, L. Karlsson, and R. Feifel, Phys. Rev. A **82**, 043418 (2010).
[18] P. Lablanquie, M. A. Khalal, L. Andric, J. Palaudoux, F. Penent, J.-M. Bizau, D. Cubaynes, K. Jänkälä, Y. Hikosaka, K. Ito, K. Bučar, and M. Žitnik, J. Electron Spectrosc. Relat. Phenom. **220**, 125 (2017).
[19] M. Žitnik, R. Püttner, G. Goldsztejn, K. Bučar, M. Kavčič, A. Mihelič, T. Marchenko, R. Guillemin, L. Journel, O. Travnikova, D. Céolin, M. N. Piancastelli, and M. Simon, Phys. Rev. A **93**, 021401(R) (2016).
[20] O. Travnikova, T. Marchenko, G. Goldsztejn, K. Jänkälä, N. Sisourat, S. Carniato, R. Guillemin, L. Journel, D. Céolin, R. Püttner, H. Iwayama, E. Shigemasa, M. N. Piancastelli, and M. Simon, Phys. Rev. Lett. **116**, 213001 (2016).
[21] M. H. Chen, Phys. Rev. A **44**, 239 (1991).
[22] D. Coster and R. D. L. Kronig, Physica (Amsterdam) **2**, 13 (1935).
[23] M. Sacchi, N. Jaouen, H. Popescu, R. Gaudemer, J. M. Tonnerre, S. G. Chiuzbaian, C. F. Hague, A. Delmotte, J. M. Dubuisson, G. Cauchon, B. Lagarde, and F. Polack, J. Phys.: Conf. Ser. **425**, 072018 (2013).
[24] K. Ito, F. Penent, Y. Hikosaka, E. Shigemasa, I. H. Suzuki, J. H. D. Eland, and P. Lablanquie, Rev. Sci. Instrum. **80**, 123101 (2009).
[25] I. P. Grant, *Relativistic Quantum Theory of Atoms and Molecules: Theory and Computation* (Springer, New York, 2007).
[26] P. Jönsson, X. He, C. Froese Fischer, and I. P. Grant, Comput. Phys. Commun. **177**, 597 (2007).
[27] S. Fritzsche, Comput. Phys. Commun. **183**, 1525 (2012).
[28] T. Åberg, Phys. Rev. **156**, 35 (1967).
[29] S. Fritzsche, K. Jänkälä, M. Huttula, S. Urpelainen, and H. Aksela, Phys. Rev. A **78**, 032514 (2008).
[30] B. Kanngießer, M. Jainz, S. Brünken, W. Benten, Ch. Gerth, K. Godehusen, K. Tiedtke, P. van Kampen, A. Tutay, P. Zimmermann, V. F. Demekhin, and A. G. Kochur, Phys. Rev. A **62**, 014702 (2000).
[31] Y. Hikosaka, T. Aoto, P. Lablanquie, F. Penent, E. Shigemasa, and K. Ito, Phys. Rev. Lett. **97**, 053003 (2006).
[32] S. Svensson, N. Martensson, and U. Gelius, Phys. Rev. Lett. **58**, 2639 (1987).
[33] N. Martensson, S. Svensson, and U. Gelius, J. Phys. B: At. Mol. Phys. **20**, 6243 (1987).
[34] V. Carravetta, J. Phys. B: At., Mol. Opt. Phys. **21**, 1777 (1988).
[35] V. G. Yarzhemsky, M. Ya. Amusia, and L. V. Chernysheva, J. Electron Spectrosc. Relat. Phenom. **127**, 153 (2002).
[36] L. Young, E. P. Kanter, B. Krässig, Y. Li, A. M. March, S. T. Pratt, R. Santra, S. H. Southworth, N. Rohringer, L. F. DiMauro, G. Doumy, C. A. Roedig, N. Berrah, L. Fang, M. Hoener, P. H. Bucksbaum, J. P. Cryan, S. Ghimire, J. M. Glownia, and D. A. Reis *et al.*, Nature **466**, 56 (2010).
[37] P. Salén, P. van der Meulen, H. T. Schmidt, R. D. Thomas, M. Larsson, R. Feifel, M. N. Piancastelli, L. Fang, B. Murphy, T. Osipov, N. Berrah, E. Kukk, K. Ueda, J. D. Bozek, C. Bostedt, S. Wada, R. Richter, V. Feyer, and K. C. Prince, Phys. Rev. Lett. **108**, 153003 (2012).
[38] R. A. Mori, E. Paris, G. Giuli, S. G. Eeckhout, M. Kavčič, M. Žitnik, K. Bučar, L. G. M. Pettersson, and P. Glatzel, Inorg. Chem. **49**, 6468 (2010).